Kinetic Monte Carlo for Process Simulation: First Principles Calibrated Parameters for BO_2

Pierre-Louis Julliard
STMicroelectronics
Crolles, France
pierre-louis.julliard@st.com

Antoine Jay
LAAS-CNRS
Toulouse, France
ajay@laas.fr

Miha Gunde
LAAS-CNRS
Toulouse, France
miha.gunde@laas.fr

Nicolas Salles
CNR-IOM
Trieste, Italy
salles@iom.cnr.it

Frederic Monsieur
STMicroelectronics
Crolles, France
frederic.monsieur@st.com

Nicolas Guitard
STMicroelectronics
Crolles, France
nicolas.guitard@st.com

Thomas Cabout
STMicroelectronics
Crolles, France
thomas.cabout@st.com

Sylvain Joblot
STMicroelectronics
Crolles, France
sylvain.joblot@st.com

Layla Martin-Samos
CNR-IOM
Trieste, Italy
marsamos@iom.cnr.it

Denis Rideau
STMicroelectronics
Crolles, France
denis.rideau@st.com

Fuccio Cristiano
LAAS-CNRS
Toulouse, France
cfuccio@laas.fr

Anne Hemeryck
LAAS-CNRS
Toulouse, France
anne.hemeryck@laas.fr

***Abstract*—The formation energies and diffusion paths of O_i, O_{2i} and BO_2 complex in silicon are determined using *ab initio* calculations and used to calibrate a Kinetic Monte Carlo. The aim is to simulate the formation of the BO_2 complex in Technology Computer Aided Design tools.**

***Index Terms*—Boron-Oxygen complex, Kinetic Monte Carlo, process simulation, TCAD**

I. Introduction

Formation of Boron-Oxygen complex (BO_2) is known to be a major issue in Cz-silicon photovoltaic cells: the BO_2 induces a drastic reduction of the minority lifetime carrier [1], which is detrimental for the photoconversion efficiency. It is also detrimental in image sensors since BO_2 is reported to introduce a deep energy level into the bandgap [2] that can act as an active recombination center giving rise to a significant increase of the dark current. As reported in [3] optimizing the process can avoid the formation of BO_2 complex.

The purpose of this study is first to identify the fundamental mechanisms underlying the formation of BO_2 complex in silicon material by means of ab initio calculations. And later, to exploit the results to accurately calibrate the Sentaurus Process KMC solver [4]. It will be shown that BO_2 complex formation requires a detailed description of the diffusion of isolated oxygen O_i, the formation and possible dissociation of O_{2i}, and the association and dissociation of O_{2i} with the Boron doping element as detailed in Section III-A. In Section III-B, with the new first principle-based parameters, the solver predicts diffusion coefficients in better agreement with available experimental data.

978-1-6654-0685-7/21/$31.00

II. Simulation and calibration method

Each KMC event is governed by an Arrhenius' law $D \times exp(E_{ac}/k_BT)$ that requires the knowledge of its entropic prefactor D and of its activation barrier E_{ac}.

The events needed to form the BO_2 complex, are the diffusion of isolated O_i atoms, their agglomeration in molecular O_{2i} and the formation of BO_2. Hence, four species have to be implemented in the KMC code: O_i, O_{2i}, B_sO_{2i} and B_iO_{2i}, where B_sO_{2i} and B_iO_{2i} respectively refer to a BO_2 complex in which the boron atom is in a substitutional [5] and interstitial site [6].

These species have been relaxed in a 216-atoms cubic supercell of silicon atoms with periodic boundary conditions in different charge states until forces on each atom are less than 10^{-4} Ry/a.u. Based on the formation energy of such species, we identify the one most likely to exist in the material and which will be likely to migrate [6]. Total energy calculations have been performed within Density Functional Theory (DFT) [7], [8] using the Perdew-Burke-Ernzerhof functional (PBE [9]) as implemented in Quantum Espresso [10]. The Heyd-Scuseria-Ernzerhof (HSE [11]) functional has been used for the evaluation of the formation energy at each charge state. PAW and Vanderbilt pseudopotentials were used for the PBE and for the HSE calculations, respectively. The plane-wave basis cut-off was set to 50 Ry. The sample of the Brillouin zone was performed at the Γ point only with PBE and with a Monkhorst-Pack [12] grid of 2^3 **k**-points for the HSE. Activation barriers E_{ac} have been determined using ARTn refine-saddle mode [13]. D have been fitted to match the diffusion coefficients measured in [14] [15]. Binding energy E_b for a given system is determined with the difference

between the formation energy E_f of the system and the formation energies of the elements composing the system isolated in a Si-supercell: $E_b(O_{2i}) = E_f(O_{2i}) - 2 \times E_f(O_i)$.

III. Results

A. DFT Investigation

O_i specie: formation and migration - We found that the most stable structure for O_i is the C_{1h}, in agreement with [16] (O_i-A in Fig. 1.A). The charge state is found to be neutral independently of the Fermi level value as shown in Fig. 1. The calculated migration energy for O_i is 2.25 eV. The saddle point of the migration is shown in Fig. 1.B. Experimentally, the high temperature diffusion of O_i species in silicon is associated to a migration barrier of 2.53 eV [17].

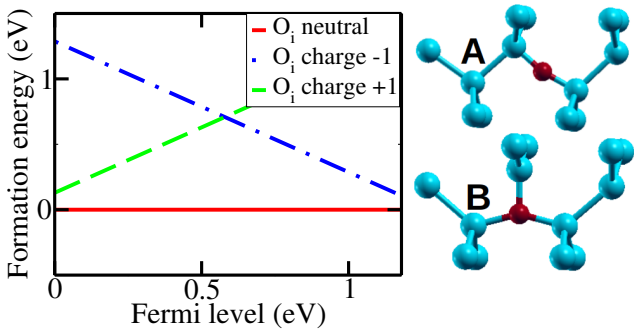

Fig. 1. Left: O_i formation energy for different charge states. Right: Atomic configuration for C_{1h} (O_i-A) and saddle point of migration path (O_i-B). Red and blue spheres are respectively O and Si atoms.

O_{2i} specie: formation, dissociation and migration - Staggered O_{2i}-st and O_{2i}^{++} squared configurations are the most discussed structures discussed in the literature [18]. In our calculations, the staggered O_{2i}-st configuration (Fig. 2 top-right) exhibits the lowest energy (Fig. 2 top-left) in comparison to the formation energy of the O_{2i}^{++} squared structure (O_{2i}-sq in Fig.2). Therefore the hypothesis of a migration by the means of O_{2i}^{++} squared structure found in [18] is unlikely to occur even at low Fermi level energy. The migration energy is thus calculated for a neutral charge state. The barrier energy is calculated to be 1.40 eV. O_{2i}-sq is revealed to be the saddle point along the migration path. Binding energy of O_{2i} (-0.30 eV) calculated with PBE is consistent with experimental values (Tab. I) and indicates that the formation of molecular O_{2i} specie is a favorable process.

TABLE I
Comparison of the calculated activation barriers E_{ac} and binding energy E_b (in eV) and the experimental ones. The prefactor D (s^{-1}) is adjusted empirically to fit experimental data from [14] [15].

	DFT-PBE			Exp.	
	E_{ac}	E_b	D	E_{ac}	E_b
O_i	2.25	-	3.10^{14}	2.53 [17]	-
O_{2i}	1.40	-0.30	4.10^{15}	1.5 [15]	-0.30 [19]

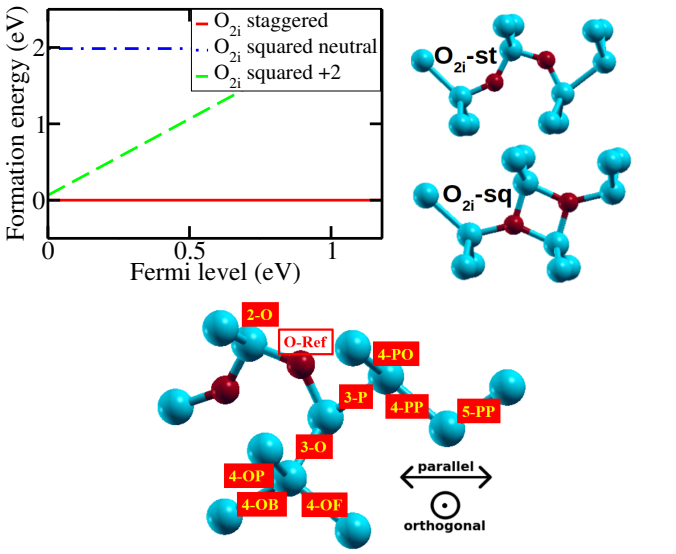

Fig. 2. Top left: O_{2i} formation energy for squared (O_{2i}-sq) and staggered (O_{2i}-st) structures in different charge states. Top right: O_{2i}-st atomic configuration. O_{2i}-sq is the saddle point of migration path of O_{2i}-st. Bottom: Mapping of the local environment involved during the dissociation of the O_{2i}-st toward the formation of two isolated O_i. Red boxes represent the different interstitial sites where O_i from O-Ref can migrate. The number and the letter in the boxes indicate the distance between Si neighbors and the direction of the migration (P Parallel, O Orthogonal) respectively. Corresponding activation barriers are given in Tab. II.

An exhaustive characterization of the activation barriers of the dissociation/association mechanisms of O_{2i}-st is necessary to correctly identify, then predict and simulate at what temperature O_{2i}-st is formed and how often it dissolves. To understand the interaction between the oxygen atoms and how it affects the activation barriers, one O_i atom is taken away from the atomic configuration O_{2i}-st to the next interstitial sites as depicted in Fig. 2 bottom panel. All the energy barriers associated to the dissociation mechanisms of the O_{2i}-st as a function of the nearest neighbors influence are given in Tab. II. Note that the calculated activation barriers associated to the energy gains provided in Tab. II allow a description of the formation of O_{2i}-st from two isolated O_i according to back reactions. Such an approach is carried out until the total energy of the system is equal to that of two isolated oxygen atoms, meaning that the two atoms are no longer in interaction, *i.e.* until the fourth Si neighbors.

To dissociate O_{2i}-st, we observe that the activation barriers of diffusion occurring in the direction parallel to the two O atoms of structure O_{2i}-st are always smaller than in the other direction: O_i initially on O-Ref will successively migrate toward sites 3-P, 4-PP... The reorientation of the structure O_{2i}-st on another plane (O_i on site O-Ref moving to site 2-O on Fig. 2) requires a larger activation barrier of 2.45 eV. We reveal that the diffusion of O_{2i}-st is highly anisotropic. In the fourth neighbor position, the O_i atoms are still influencing each other. In this zone where the two O_i atoms interact, the two O_i atoms will have to tendency to cluster to form the

TABLE II

ACTIVATION BARRIERS (E_{ac}) FOR THE DISSOCIATION OF O_{2i}-ST REFERRING TO CONFIGURATIONS LABELLED IN FIG. 2 BOTTOM PANEL. ΔE IS THE ENERGY DIFFERENCE BETWEEN THE INITIAL AND FINAL CONFIGURATIONS. ENERGIES ARE IN EV.

From O-Ref to		
site	E_{ac}	ΔE
2-O	2.45	0.00
3-P	1.82	0.60
3-O	2.12	0.14

From site 3-O to		
site	E_{ac}	ΔE
4-OP	2.24	0.17
4-OF	2.36	-0.10
4-OB	2.28	0.06

From site 3-P to		
site	E_{ac}	ΔE
4-PP	1.38	-0.12
4-PO	1.67	0.48

From site 4-P to		
site	E_{ac}	ΔE
5-PP	1.67	-0.03

O_{2i}-st, rather than to separate. Beyond this interaction limit, the behavior of oxygen can be considered as an isolated O_i atom.

For an accurate predictive modeling of O_{2i}-st dissociation, we demonstrate the importance of considering the existing interaction between oxygen atoms even at long distances. We also identify the interaction limit of these oxygen atoms. Furthermore, this DFT-based study reveals that the dissociation (and formation) is highly anisotropic, which could be critical in the thermally activated regime.

BO_2 complex: stability and formation - Structural relaxations confirm that the more stable configurations for BO_2 complex are the B_sO_{2i} and B_iO_{2i} defects as obtained in [5] and [6]. Formation energies for the B_sO_{2i} defect demonstrate that the B_sO_{2i} in B configuration is dominant for a Fermi level below 0.22 eV whereas the A configuration is more stable above (Fig. 3).

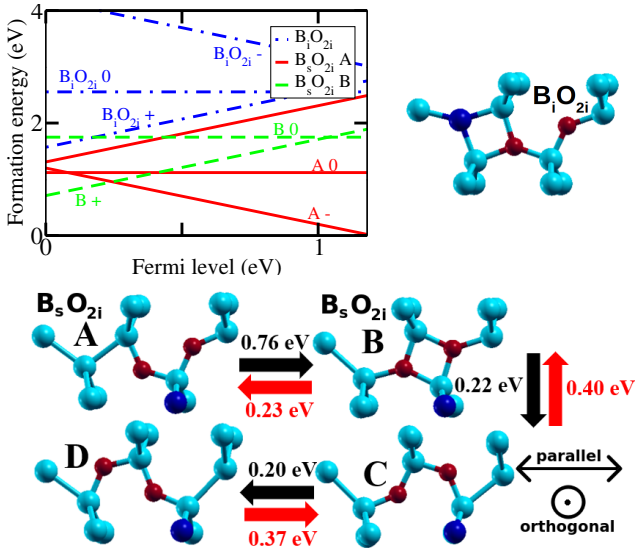

Fig. 3. Top left: formation energies for B_sO_{2i} and B_iO_{2i} in their more favorable charge state. Top right : atomic configuration of B_iO_{2i}. Bottom: Minimum Energy Path of the migration of O_{2i}-st from a B_sO_{2i} complex (A). Boron atoms are represented by dark blue spheres.

In the following, we focus on the B_sO_{2i} complex formation. This structure is likely to have a high migration barrier because of the stability of the boron atom in a substitutional position. Boron diffusion is only shown when associated with the presence of a vacancy [20]. Then, comparing the total energy between the B_sO_{2i} in configuration A and isolated O_{2i}-st and B_s^- configuration indicates that the formation of B_sO_{2i} is a favorable process (-1.09 eV).

We consider that the dissociation of the B_sO_{2i} complex occurs through the departure of O_{2i} from the B_sO_{2i} complex. As in the case of O_{2i}, a detailed study of the dissociation of B_sO_{2i} should be investigated as a function of the interaction distance between O_{2i} and B atom. Because of the large number of possibilities for dissociation, based on the findings of O_{2i} diffusion described previously, we initially assume that O_{2i} diffusion occurs in the plane containing the two oxygen atoms (in the P direction), consistent with other study [5]. The minimum energy path of the corresponding migration is shown in Fig. 3-Bottom part. The activation barrier to transform the B_sO_{2i}-A configuration into the B_sO_{2i}-B configuration (when O_{2i} is no longer symmetric about the B atom) is large by 0.76 eV. Once the complex is in the B_sO_{2i}-B configuration, the dissociation of B_sO_{2i}-B is slightly in favor of the formation of B_sO_{2i}-C (E_{ac} are 0.22 eV from B to C *vs.* 0.23 eV from B to A). The same trend is observed in the next step between the B_sO_{2i}-C and B_sO_{2i}-D configuration (E_{ac} are 0.20 eV from C to D *vs.* 0.40 eV from C to B). Thus these calculations are consistent with the formation of the B_sO_{2i}-A configuration, which once formed is very stable. The formation of this complex is nevertheless dependent on the area around the Boron atom which tends to make this complex not form immediately. This formation time linked to the tendency of O_{2i} not to be systematically attracted by the boron atom, must be considered to give a predictive account of the formation of B_sO_{2i}.

B. KMC process simulation

O_i and O_{2i} calibration - For this purpose we calculated the oxygen diffusivity with the view of comparing KMC prediction to measurement of [14] and [15]. Oxygen diffusivity is simulated with KMC by following the diffusion of a buried oxygen-rich silicon layer in a bulk silicon during annealing at different temperatures. Oxygen diffusion in silicon is assumed to be driven by O_i migration for temperature above 700°C. Between 400°C and 700°C, the experimental diffusivity shows an enhancement. Several hypotheses exist to explain the diffusion acceleration: a fast diffusion of O_{2i} complex is one of the most cited explanations [17].

For an efficient use, KMC codes use a single energy barrier to simulate a dissociation event. Dissociation energy for O_{2i} is determined as done in [21]: $E_{dissociation}(O_{2i}) = E_b(O_{2i}) + E_m(O_i)$. The DFT values used for the KMC calibration are given in Tab. I. As can be seen in Fig. 4, the DFT calibrated-KMC exhibits a clear enhanced diffusion between 400°C and 700°C. We notice a discrepancy between the experimental data and the KMC simulations results, especially in the region

of the enhanced diffusion. This observation can have several explanations. The O_{2i} driven diffusion is dependent on the migration energy of the O_{2i}-st but also on its interaction not favoring the dissociation of O_{2i}. As we detailed in previous section, the multiple pathways shown in Fig. 2 should be considered to better represent the diffusion of O_{2i}. A single dissociation and migration event is certainly not sufficient to accurately describe the increased diffusion.

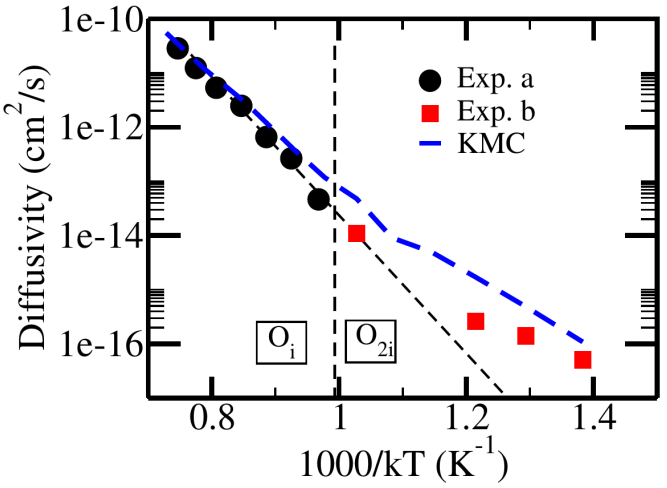

Fig. 4. KMC prediction for oxygen diffusivity obtained with the events of Table I. Comparison with the experimental diffusion coefficients from [14] (a) and [15] (b). Dashed vertical line shows the separation between the O_i driven diffusion regime and the O_{2i} diffusion regime and dashed inclined line is guideline for the eyes for the O_i mediated diffusion.

Implementation of B_sO_{2i} complex - It can be noted incidentally that the boron parameters have been calibrated elsewhere [21]. To implement the BO_2 complex formation, following method could be applied: the emission of an O_{2i} from a B_sO_{2i} defect can be estimated using the same method as the emission of an O_i from an O_{2i}, by knowing the energies of the B atoms and O_{2i} in a Si supercell. In such way, the dissociation mechanism to form a B_s^- and an O_{2i} from a negatively charged A configuration of B_sO_{2i} must overcome a binding energy of 1.09 eV and the migration energy of the O_{2i} given in Tab I. These two barriers lead to an activation energy of 2.49 eV for the dissociation mechanism.

As we have already proven before, this calibration method has again several limitations. A KMC code that uses only one activation barrier per event cannot adequately handle the effect of the interactions at more or less long distance that we observe for the dissociation (or formation) of the B_sO_{2i} complex.

IV. Conclusion

DFT calculations provide accurate values of activation energies for atomistic events as needed for TCAD tool calibration. The KMC calibrated with *ab initio* inputs reproduces enhanced diffusion of oxygen by the mean of O_{2i} kinetics. We also show that by a conventional way, it is also possible to implement the process simulation of the BO_2 formation using the DFT calculated parameters for oxygen species and BO_2.

In the idea of calibrating the KMC sentaurus code as built today, we have proposed in this paper the possibility of implementing a single activation barrier as required by the code that we have calculated in DFT. This approach has the advantage of being fast and easy to use. However, we showed through a detailed study at the ab initio scale, that this approach has many drawbacks.

To solve this problem, an off-lattice KMC seems to be a promising tool. We are currently developing such an off lattice KMC [22] in order to use the complete library of possible events we have identified in this paper. The goal of the off lattice KMC simulations will be to determine the correct prefactor as calculated in DFPT [23] and avoid its fitting on the experimental data. The objective of this KMC will also be to account for the disparity of all activation barriers calculated above. It will then be necessary to determine lifetimes for each of these configurations, to construct energy basins, for simpler, more efficient but accurate implementation in commercial TCAD tools, such as using and refining a single activation barrier for both migration and dissociation mechanisms.

V. Acknowledgements

This work was performed using HPC resources from CALMIP-Grant P1555. The research leading to these results has received funding from the European Union's Horizon 2020 research and innovation program under grant agreement No. 871813 MUNDFAB. A. Jay, M. Gunde, N. Salles, L. Martin-Samos and A. Hémeryck are active members of the Multiscale and Multi-Model Approach for Materials in Applied Science consortium (MAMMASMIAS consortium), and acknowledge the efforts of the consortium in fostering scientific collaboration.

References

[1] S. Glunz, S. Rein, W. Warta, J. Knobloch, and W. Wettling, "On the degradation of cz-silicon solar cells," in *Proc. 2nd WC PVSEC*, 1998.

[2] T. Mchedlidze and J. Weber, "Direct detection of carrier traps in si solar cells after light-induced degradation," *physica status solidi (RRL)–Rapid Research Letters*, vol. 9, no. 2, pp. 108–110, 2015.

[3] X. Yu, P. Wang, P. Chen, X. Li, and D. Yang, "Suppression of boron–oxygen defects in p-type czochralski silicon by germanium doping," *Appl. Phys. Lett.*, vol. 97, no. 5, p. 051903, 2010.

[4] "Sentaurus process user guide, 2019.03, synopsis inc."

[5] M. Vaqueiro-Contreras, V. P. Markevich, J. Coutinho, P. Santos, I. F. Crowe, M. P. Halsall, I. Hawkins, S. B. Lastovskii, L. I. Murin, and A. R. Peaker, "Identification of the mechanism responsible for the boron oxygen light induced degradation in silicon photovoltaic cells," *J. App. Phys.*, vol. 125, no. 18, p. 185704, 2019.

[6] X. Chen, X. Yu, X. Zhu, P. Chen, and D. Yang, "First-principles study of interstitial boron and oxygen dimer complex in silicon," *Applied Physics Express*, vol. 6, no. 4, p. 041301, 2013.

[7] P. Hohenberg and W. Kohn, "Inhomogeneous electron gas," *Phys. Rev.*, vol. 136, p. B864, 1964.

[8] W. Kohn and S. L. J, "Self-consistent equations including exchange and correlation effects," *Phys. Rev.*, vol. 140, p. A1133, 1965.

[9] J. P. Perdew, K. Burke, and M. Ernzerhof, "Generalized gradient approximation made simple," *Phys. Rev. Let.*, vol. 77, no. 18, p. 3865, 1996.

[10] P. Giannozzi, S. Baroni, N. Bonini, M. Calandra, R. Car, C. Cavazzoni, D. Ceresoli, G. L. Chiarotti, M. Cococcioni, I. Dabo, A. Dal Corso, S. de Gironcoli, S. Fabris, G. Fratesi, R. Gebauer, U. Gerstmann, C. Gougoussis, A. Kokalj, M. Lazzeri, L. Martin-Samos, N. Marzari, F. Mauri, R. Mazzarello, S. Paolini, A. Pasquarello, L. Paulatto, C. Sbraccia, S. Scandolo, G. Sclauzero, A. P. Seitsonen, A. Smogunov, P. Umari, and R. M. Wentzcovitch, "Quantum espresso: a modular and open-source software project for quantum simulations of materials," *J. Phys.: Cond. Matter.*, vol. 21, p. 395502, 2009.

[11] J. Heyd, G. E. Scuseria, and M. Ernzerhof, "Hybrid functionals based on a screened coulomb potential," *J. Chem. Phys.*, vol. 118, no. 18, pp. 8207–8215, 2003.

[12] H. Monkhorst and J. Pack, "Special points for Brillouin-zone integrations," *Phys. Rev. B*, vol. 13, p. 5188, 1976.

[13] A. Jay, C. Huet, N. Salles, M. Gunde, L. Martin-Samos, N. Richard, G. Landa, V. Goiffon, S. De Gironcoli, A. Hémeryck, and N. Mousseau, "Finding reaction pathways and transition states: r-artn and d-artn as an efficient and versatile alternative to string approaches," *J. Chem. Theory Comput.*, vol. 16, pp. 6726–6734, 2020.

[14] F. Livingston, S. Messoloras, R. Newman, B. Pike, R. Stewart, M. Binns, W. Brown, and J. Wilkes, "An infrared and neutron scattering analysis of the precipitation of oxygen in dislocation-free silicon," *Journal of Physics C: Solid State Physics*, vol. 17, no. 34, p. 6253, 1984.

[15] Z. Zeng, J. Murphy, R. Falster, X. Ma, D. Yang, and P. Wilshaw, "The effect of impurity-induced lattice strain and fermi level position on low temperature oxygen diffusion in silicon," *J. App. Phys.*, vol. 109, no. 6, p. 063532, 2011.

[16] J. Coutinho, R. Jones, P. Briddon, and S. Öberg, "Oxygen and dioxygen centers in si and ge: Density-functional calculations," *Phys. Rev. B*, vol. 62, no. 16, p. 10824, 2000.

[17] R. Newman, "Oxygen diffusion and precipitation in czochralski silicon," *J. Phys.: Cond. Matter.*, vol. 12, no. 25, p. R335, 2000.

[18] M.-H. Du, H. M. Branz, R. S. Crandall, and S. Zhang, "Bistability-mediated carrier recombination at light-induced boron-oxygen complexes in silicon," *Phys. Rev. Let.*, vol. 97, no. 25, p. 256602, 2006.

[19] L. Murin, T. Hallberg, V. Markevich, and J. Lindström, "Experimental evidence of the oxygen dimer in silicon," *Phys. Rev. Let.*, vol. 80, no. 1, p. 93, 1998.

[20] D. Tsoukalas and P. Ciienevier, "Boron diffusion in silicon by a vacancy mechanism," *Phys. Sol. Stat.*, vol. 92, pp. 495–501, 1985.

[21] I. Martin-Bragado, P. Castrillo, M. Jaraiz, R. Pinacho, J. Rubio, and J. Barbolla, "Physical atomistic kinetic monte carlo modeling of fermi-level effects of species diffusing in silicon," *Phys. Rev. B*, vol. 72, no. 3, p. 035202, 2005.

[22] M. Gunde, N. Salles, N. Richard, A. Hemeryck, and L. Martin Samos, "An off-lattice kinetic monte carlo kernel guided by topological and geometrical analysis to bridge accurate ab-initio calculations and large scale simulations," *Bulletin of the American Physical Society*, 2021.

[23] S. Baroni, S. de Gironcoli, A. Dal Corso, and P. Giannozzi, "Phonons and related crystal properties from density-functional perturbation theory," *Rev. Mod. Phys.*, vol. 73, p. 515, 2001.